

1  
2  
3  
4  
5  
6  
7  
8  
9  
10  
11  
12  
13  
14  
15  
16  
17  
18  
19  
20  
21  
22  
23  
24  
25  
26  
27  
28  
29  
30  
31  
32  
33  
34

## Increased Resistance of SARS-CoV-2 Variant P.1 to Antibody Neutralization

Pengfei Wang<sup>1\*+</sup>, Ryan G. Casner<sup>2\*</sup>, Manoj S. Nair<sup>1\*</sup>, Maple Wang<sup>1</sup>, Jian Yu<sup>1</sup>, Gabriele Cerutti<sup>2</sup>, Lihong Liu<sup>1</sup>, Peter D. Kwong<sup>2,3</sup>, Yaoxing Huang<sup>1</sup>, Lawrence Shapiro<sup>1,2+</sup>, & David D. Ho<sup>1,4,5,6+</sup>

<sup>1</sup>Aaron Diamond AIDS Research Center, Columbia University Vagelos College of Physicians and Surgeons, New York, NY 10032, USA. <sup>2</sup>Department of Biochemistry and Molecular Biophysics, Columbia University, New York, NY 10032, USA. <sup>3</sup>Vaccine Research Center, National Institutes of Health, Bethesda, MD 20892, USA. <sup>4</sup>Department of Microbiology and Immunology, Columbia University Irving Medical Center, New York, NY 10032, USA. <sup>5</sup>Division of Infectious Diseases, Department of Internal Medicine, Columbia University Vagelos College of Physicians and Surgeons, New York, NY 10032, USA. <sup>6</sup>Lead contact. \*These authors contributed equally. <sup>+</sup>Address correspondence to [pw2517@cumc.columbia.edu](mailto:pw2517@cumc.columbia.edu), [lss8@columbia.edu](mailto:lss8@columbia.edu), or [dh2994@cumc.columbia.edu](mailto:dh2994@cumc.columbia.edu)

35 **SUMMARY**

36 **The relative resistance of SARS-CoV-2 variants B.1.1.7 and B.1.351 to antibody**  
37 **neutralization has been described recently. We now report that another emergent**  
38 **variant from Brazil, P.1, is not only refractory to multiple neutralizing monoclonal**  
39 **antibodies, but also more resistant to neutralization by convalescent plasma (3.4**  
40 **fold) and vaccinee sera (3.8-4.8 fold). The cryo-electron microscopy structure of**  
41 **a soluble prefusion-stabilized spike reveals the P.1 trimer to adopt exclusively a**  
42 **conformation in which one of the receptor-binding domains is in the “up”**  
43 **position, with the functional impact of mutations appearing to arise from local**  
44 **changes instead of global conformational alterations. The P.1 variant threatens**  
45 **current antibody therapies but less so the protective efficacy of our vaccines.**

46  
47 SARS-CoV-2 P.1, emerging from the B.1.1.28 lineage, has become a dominant variant  
48 in Brazil (Faria, 2021; Naveca, 2021). P.1 contains 10 spike mutations in addition to  
49 D614G, including K417T, E484K, and N501Y in the receptor-binding domain (RBD),  
50 L18F, T20N, P26S, D138Y and R190S in the N-terminal domain (NTD), and H655Y  
51 near the furin cleavage site. This new variant could threaten the efficacy of current  
52 monoclonal antibody (mAb) therapies or vaccines, because it shares mutations at the  
53 same three RBD residues with B.1.351, a variant that first emerged from South Africa  
54 (Tegally et al., 2021). We and others (Liu et al., 2021; Wang et al., 2021; Wu et al.,  
55 2021) have shown that B.1.351 is more resistant to neutralization by some mAbs,  
56 convalescent plasma, and vaccinee sera, in part due to a E484K mutation that also  
57 exists in P.1. We therefore obtained the P.1 authentic virus and also created, as

58 previously described (Liu et al., 2020; Wang et al., 2020; Wang et al., 2021), a VSV-  
59 based SARS-CoV-2 pseudovirus with all 10 mutations of the P.1 variant (BZΔ10), and  
60 assessed their susceptibility to neutralization by 18 neutralizing mAbs, 20 convalescent  
61 plasma, and 22 vaccinee sera as previously reported (Wang et al., 2021).

62

63 We first assayed the neutralizing activity of four mAbs with emergency use authorization  
64 (EUA), including REGN10987 (imdevimab), REGN10933 (casirivimab) (Hansen et al.,  
65 2020), LY-CoV555 (bamlanivimab) (Chen et al., 2021; Gottlieb et al., 2021), and CB6  
66 (etesevimab) (Gottlieb et al., 2021; Shi et al., 2020) against P.1 pseudovirus (BZΔ10)  
67 and authentic virus, alongside with their wildtype (WT or WA1) counterparts. As shown  
68 in Figure 1A (left panel) and Figure S1A, the neutralizing activities of three of the mAbs  
69 with EUA were markedly or completely abolished against P.1. The only mAb with EUA  
70 retaining its activity was REGN10987. We next tested the neutralizing activity of eight  
71 additional RBD mAbs, including ones from our own collection (2-15, 2-7, 1-57, & 2-36)  
72 (Liu et al., 2020) as well as S309 (Pinto et al., 2020), COV2-2196 & COV2-2130 (Zost et  
73 al., 2020), and C121 (Robbiani et al., 2020). The neutralizing activities of the two potent  
74 mAbs targeting the receptor-binding motif, 2-15 and C121, were completely lost against  
75 P.1 (Figure 1A, middle panel, and Figure S1A). Other mAbs targeting the “inner side” or  
76 the “outer side” of RBD retained their activities against P.1, however. Overall, the data  
77 on pseudovirus and authentic virus were in agreement, and the findings on P.1 mimic  
78 those observed for B.1.351 (Wang et al., 2021), which should not be surprising since  
79 the triple RBD mutations in P.1 and B.1.351 are largely the same.

80

81 We also assessed the neutralizing activity of six NTD mAbs (Liu et al., 2020) against the  
82 P.1 pseudovirus and authentic virus (Figure 1A, right panel; and Figure S1B). P.1 was  
83 profoundly resistant to neutralization by four NTD antibodies: 2-17, 4-18, 4-19, and 5-7.  
84 Interestingly, 5-24 and 4-8, two mAbs targeting the antigenic supersite in NTD (Cerutti  
85 et al., 2021) that have completely lost neutralizing activity against B.1.351 (Wang et al.,  
86 2021), remained active against P.1. To understand the specific mutations responsible  
87 for the observed pattern of neutralization, we then tested these NTD mAbs against a  
88 panel of pseudoviruses, each containing only a single NTD mutation found in P.1  
89 (Figure S1B). As expected, 5-24 and 4-8 retained activity against all single-mutation  
90 pseudoviruses. P26S only partially accounted for the loss of activity of 4-18; L18F,  
91 T20N, and D138Y contributed to the loss of activity of 2-17 and 4-19; and L18F, T20N,  
92 D138Y, and R190S together resulted in the loss of activity of 5-7.

93  
94 We also examined a panel of convalescent plasma obtained from 20 SARS-CoV-2  
95 patients infected in the Spring of 2020, as previously reported (Wang et al., 2021).  
96 Each plasma sample was assayed for neutralization against the P.1 pseudovirus and  
97 authentic virus in parallel with their WT counterparts. As shown in Figure S1C, many  
98 samples lost >2-fold neutralizing activity against BZΔ10 and P.1. The magnitude of the  
99 drop in plasma neutralization ID50 titers is summarized in Figure 1B (left panel),  
100 showing a 6.5-fold loss of activity against the variant pseudovirus and a 3.4-fold loss of  
101 activity against the authentic virus.

102

103 Twenty-two vaccinee sera were obtained, as previously reported (Wang et al., 2021),  
104 from 12 individuals who received Moderna SARS-Co-2 mRNA-1273 Vaccine (Anderson  
105 et al., 2020) and 10 individuals who received the Pfizer BNT162b2 Covid-19 Vaccine  
106 (Polack et al., 2020). Each serum sample was assayed for neutralization against  
107 BZΔ10 and P.1 together with WT viruses. The extent of the decline in neutralization  
108 activity is summarized in Figure 1B (middle and right panels), and each neutralization  
109 profile is shown in Figure S1D. A loss of activity against BZΔ10 and P.1 was noted for  
110 every sample, but the magnitude of the loss was modest (2.2-2.8 fold for the  
111 pseudovirus; 3.8-4.8 fold for the authentic virus) and not as striking as was observed  
112 against B.1.351 (6.5-8.6 fold for pseudovirus; 10.3-12.4 fold for authentic virus) (Wang  
113 et al., 2021).

114  
115 To provide insight into the mechanisms of antibody resistance, we determined the  
116 structure of the 2-proline-stabilized P.1 spike protein at 3.8 Å resolution by single-  
117 particle cryo-EM reconstruction (Figures 2 and S2, Table S1). Overall, the structure of  
118 the P.1 spike was highly similar to the D614G variant (Korber et al., 2020; Yurkovetskiy  
119 et al., 2020) with 3D classes observed only for the single-RBD-up conformation. This  
120 was expected, as the D614G mutation, contained in P1, appears to favor the one-up  
121 orientation of RBD, which is required for ACE2 binding and recognition by some RBD-  
122 directed antibodies. Structural mobility was observed with the raised RBD (protomer B),  
123 but not with protomers A and C, which were in the down orientation (Video S1). Map  
124 density was well satisfied by the previously reported single-up structure (PDB 6XM0) for  
125 the majority of the trimer, except in three regions. Residues 310-322 in protomer B

126 traced a different path; residues 623-632 were disordered in protomers A and B, and  
127 partially ordered in protomer C; and residues 828-853 were disordered in protomers A  
128 and C, and partially ordered in protomer B. Notably, two of these regions around  
129 residues 320 and 840 were previously observed to “refold” between the single-up and  
130 the low-pH all-RBD-down conformation (Zhou et al., 2020), suggesting these regions  
131 are generally more mobile – and in this case, sensitive to mutation-induced  
132 conformational changes.

133  
134 Because of the high overall conformational similarity to the D614G structure, we infer  
135 the functional impact of the P.1 mutation to arise primarily from local changes in  
136 structure. Other than H655Y and T1027I, all of the mutations occur within NTD or RBD,  
137 which are the targets of neutralizing antibodies. For NTD, the N-terminus was  
138 disordered until residue 27, so we were unable to visualize mutations at residue 18, 20,  
139 and 26. Mutation D138Y is located in the center of the NTD supersite (Cerutti et al.,  
140 2021), explaining its impact on NTD antibodies 2-17 and 4-19 (Fig. S1B), whereas  
141 R190S is mostly occluded from the NTD surface (Fig. 2B). For RBD, the three  
142 mutations at K417T, E484K and N501Y are all located in the ACE2-binding region and  
143 overlap epitopes for multiple neutralizing antibodies. Their relatively equal spatial  
144 separation (Fig. 2C) allow them to impact a substantial portion of the ACE2-binding  
145 surface.

146  
147 Overall, the SARS-CoV-2 P.1 variant is of concern because of its rapid rise to  
148 dominance as well as its extensive spike mutations, which could lead to antigenic

149 changes detrimental to mAb therapies and vaccine protection. Here we report that P.1  
150 is indeed resistant to neutralization by several RBD-directed mAbs, including three with  
151 EUA. The major culprit is the E484K mutation, which has emerged independently in  
152 over 50 lineages, including in B.1.526 that we (Annavajhala et al., 2021) and others  
153 (West et al., 2021) have identified in New York recently. As for the NTD-directed mAbs,  
154 the resistance profiles are markedly different between P.1 and B.1.351, reflecting their  
155 distinct sets of mutations in NTD. Both convalescent plasma and vaccinee sera show a  
156 significant loss of neutralizing activity against P.1, but the diminution is not as great as  
157 that reported against B.1.351 (Garcia-Beltran et al., 2021; Wang et al., 2021).  
158 Therefore, the threat of increased re-infection or decreased vaccine protection posed by  
159 P.1 may not be as severe as B.1.351. Finally, given that the RBD mutations are largely  
160 the same for these two variants, the discrepancy in their neutralization susceptibility to  
161 polyclonal plasma or sera suggests that NTD mutations can have a significant effect on  
162 the susceptibility of SARS-CoV-2 to antibody neutralization.

163  
164 **Acknowledgements.** The following reagent was obtained through BEI Resources,  
165 NIAID, NIH: SARS-Related Coronavirus 2, Isolate hCoV-19/Japan/TY7-503/2021 (Brazil  
166 P.1), NR-54982, contributed by National Institute of Infectious Diseases. We thank Bob  
167 Grassucci and Chi Wang for help with cryo-EM data collection at the Columbia  
168 University cryo-EM Center at the Zuckerman Institute. This study was supported by  
169 funding from Andrew & Peggy Cherng, Samuel Yin, Barbara Picower and the JPB  
170 Foundation, Bria Biosciences, Roger & David Wu, and the Bill and Melinda Gates  
171 Foundation. Support was also provided by the Intramural Program of the Vaccine

172 Research Center, National Institute of Allergy and Infectious Diseases, National  
173 Institutes of Health.

174

175 **Author contributions.** The study was conceptualized by D.D.H. The virology  
176 experiments were carried out by P.W., M.S.N., M.W., J.Y., L.L., and Y.H. The structural  
177 experiment were carried out by R.G.C., G.C., P.D.K., and L.S. The manuscript was  
178 written by P.W., R.G.C., P.D.K., L.S., and D.D.H. and reviewed, commented, and  
179 approved by all the authors.

180

181 **Competing interests:** P.W., J.Y., M.N., Y.H., L.L., and D.D.H. are inventors on a  
182 provisional patent application on mAbs to SARS-CoV-2.

183

## 184 **Figure legends**

185 **Figure 1. Neutralization of BZΔ10 and P.1 by mAbs, convalescent plasma, and**  
186 **vaccine sera.**

187 See also Figures S1.

188 (A) Changes in neutralization IC<sub>50</sub> of select RBD and NTD mAbs.

189 (B) Changes in reciprocal plasma neutralization ID<sub>50</sub> values of convalescent plasma  
190 and reciprocal serum ID<sub>50</sub> values for persons who received Moderna or Pfizer  
191 vaccine. Mean fold change in ID<sub>50</sub> relative to the WT is written above the *p*  
192 values. Statistical analysis was performed using a Wilcoxon matched-pairs  
193 signed rank test. Two-tailed *p*-values are reported.

194

195 **Figure 2. Cryo-EM Structure of the P.1 Spike**



196 See also Figure S2 and Table S1.

197 (A) Overall cryo-EM structure of the P.1 spike trimer with domains colored as shown  
198 in key, glycans shown in green, and mutations highlighted in red. Density is  
199 shown for the 3.8 Å reconstruction with the molecular model shown in ribbon  
200 representation. The left image shows a side view, with viral membrane located  
201 below, and the right image shows the view looking down on the spike apex.

202 (B) NTD close up view.

203 (C) RBD close up view.

204

## 205 STAR METHODS

## 206 KEY RESOURCES TABLE

REAGENT or RESOURCE	SOURCE	IDENTIFIER
<b>Antibodies</b>		
2-36	Liu et al., 2020	N/A
2-15	Liu et al., 2020	N/A
2-7	Liu et al., 2020	N/A
1-57	Liu et al., 2020	N/A
4-8	Liu et al., 2020	N/A
4-18	Liu et al., 2020	N/A
5-24	Liu et al., 2020	N/A
2-17	Liu et al., 2020	N/A
4-19	Liu et al., 2020	N/A
5-7	Liu et al., 2020	N/A
REGN10987	Hansen, et al., 2020	N/A
REGN10933	Hansen, et al., 2020	N/A
LY-CoV555	Chen, et al., 2021	N/A
CB6	Shi, et al., 2020	N/A
C121	Robbiani, et al., 2020	
S309	Pinto, et al., 2020	N/A
COV2-2130	Zost, et al., 2020	N/A
COV2-2196	Zost, et al., 2020	N/A

<b>Bacterial and Virus Strains</b>		
VSV-G pseudo-typed $\Delta$ G-luciferase	Kerafast	Cat# EH1020-PM
<b>Chemicals, Peptides, and Recombinant Proteins</b>		
n-Dodecyl- $\beta$ -D-Maltopyranoside	Anatrace	Cat# D310
<b>Critical Commercial Assays</b>		
FuGENE 6	Promega	Cat# E2691
Quikchange II XL site-directed mutagenesis kit	Agilent	Cat# 200522
Luciferase Assay System	Promega	Cat# E1501
<b>Experimental Models: Cell Lines</b>		
Vero E6	ATCC	Cat# CRL-1586
HEK 293T/17	ATCC	Cat# CRL-11268
I1 mouse hybridoma	ATCC	Cat# CRL-2700
<b>Recombinant DNA</b>		
pCMV3-SARS-CoV-2-spike D614G	Wang et al., 2021	N/A
pCMV3-SARS-CoV-2-spike L18F	Wang et al., 2021	N/A
pCMV3-SARS-CoV-2-spike T20N	This study	N/A
pCMV3-SARS-CoV-2-spike P26S	This study	N/A
pCMV3-SARS-CoV-2-spike D138Y	This study	N/A
pCMV3-SARS-CoV-2-spike R190S	This study	N/A
pCMV3-SARS-CoV-2-spike BZ $\Delta$ 10	This study	N/A
<b>Deposited data</b>		
Cryo-EM structure of SARS-CoV-2 variant P.1 spike glycoprotein	This study	PDB: 7M8K EMDB: EMD-23718
<b>Software and Algorithms</b>		
GraphPad Prism Software	GraphPad Prism Software, Inc.	N/A
SerialEM	Mastronarde, 2005	<a href="https://bio3d.colorado.edu/SerialEM/">https://bio3d.colorado.edu/SerialEM/</a>
cryoSPARC	Punjani et al., 2017	<a href="https://cryosparc.com">https://cryosparc.com</a>
UCSF Chimera	Pettersen et al., 2014	<a href="https://www.cgl.ucsf.edu/chimera/">https://www.cgl.ucsf.edu/chimera/</a>
UCSF Chimera X	Pettersen et al., 2020	<a href="https://www.cgl.ucsf.edu/chimerax/">https://www.cgl.ucsf.edu/chimerax/</a>
ISOLDE	Croll, 2018	<a href="https://isolde.cimr.cam.ac.uk/">https://isolde.cimr.cam.ac.uk/</a>
Phenix	Adams et al., 2010	<a href="https://www.phenix-online.org">https://www.phenix-online.org</a>
Coot	Emsley and Cowtan, 2004	<a href="https://www2.mrc-lmb.cam.ac.uk/personal/pemsley/coot">https://www2.mrc-lmb.cam.ac.uk/personal/pemsley/coot</a>
Molprobit	Davis et al., 2004	<a href="http://molprobit.biochem.duke.edu">http://molprobit.biochem.duke.edu</a>

207

208 **RESOURCE AVAILABILITY**

209 **Lead contact**

210 Further information and requests for resources and reagents should be directed to and  
211 will be fulfilled by the Lead Contact Author David D. Ho ([dh2994@cumc.columbia.edu](mailto:dh2994@cumc.columbia.edu)).

212 **Materials availability**

213 All unique/stable reagents generated in this study are available from the Lead Contact  
214 with a completed Materials Transfer Agreement.

215 **Data and code availability**

216 Cryo-EM structure of SARS-CoV-2 variant P.1 spike glycoprotein have been deposited  
217 in the PDB (7M8K) and EMDB (EMD-23718).

218

219 **EXPERIMENTAL MODEL AND SUBJECT DETAILS**

220 **Cell lines**

221 HEK293T/17 (cat# CRL-11268) and Vero E6 cells (cat# CRL-1586) were from ATCC  
222 and cultured in 10% Fetal Bovine Serum (FBS, GIBCO cat# 16140071) supplemented  
223 Dulbecco's Modified Eagle Medium (DMEM, ATCC cat# 30-2002) at 37°C, 5% CO<sub>2</sub>. I1  
224 mouse hybridoma cells (ATCC, cat# CRL-2700) were cultured in Eagle's Minimum  
225 Essential Medium (EMEM, ATCC cat# 30-2003)) with 20% FBS.

226

227 **METHOD DETAILS**

228 **Monoclonal antibodies, patients and vaccinees**

229 Monoclonal antibodies, convalescent plasma, and vaccinee sera were the same as  
230 previously reported (Wang et al., 2021).

### 231 **Pseudovirus neutralization assays**

232 Plasmids encoding the single-mutation variants found in P.1 and 10-mutation variant  
233 (BZΔ10) were generated by Quikchange II XL site-directed mutagenesis kit (Agilent).  
234 Recombinant Indiana VSV (rVSV) expressing different SARS-CoV-2 spike variants  
235 were generated as previously described (Liu et al., 2020; Wang et al., 2020; Wang et  
236 al., 2021). Neutralization assays were performed by incubating pseudoviruses with  
237 serial dilutions of mAbs or heat-inactivated plasma or sera, and scored by the reduction  
238 in luciferase gene expression as previously described (Liu et al., 2020; Wang et al.,  
239 2020; Wang et al., 2021). Briefly, Vero E6 cells (ATCC) were seeded in 96-well plates  
240 ( $2 \times 10^4$  cells per well). Pseudoviruses were incubated with serial dilutions of the test  
241 samples in triplicate for 30 min at 37°C. The mixture was added to cultured cells and  
242 incubated for an additional 16 hrs. Luminescence was measured using Luciferase  
243 Assay System (Promega), and IC<sub>50</sub> was defined as the dilution at which the relative light  
244 units were reduced by 50% compared with the virus control wells (virus + cells) after  
245 subtraction of the background in the control groups with cells only. The IC<sub>50</sub> values were  
246 calculated using a five-parameter dose-response curve in GraphPad Prism.

### 247 **Authentic SARS-CoV-2 Microplate Neutralization**

248 The SARS-CoV-2 viruses USA-WA1/2020 (WA1), and hCoV-19/Japan/TY7-503/2021  
249 (P.1) were obtained from BEI Resources (NIAID, NIH). The deposited virus (Passage 2  
250 in Vero E6/TMPRSS2 cells) was reported to have an additional mutation as compared

251 to the clinical isolate: NSP6 (Non-structural protein 6) F184V (GISAID:  
252 EPI\_ISL\_877769). The viruses were propagated for one passage using Vero E6 cells.  
253 Virus infectious titer was determined by an end-point dilution and cytopathic effect  
254 (CPE) assay on Vero E6 cells as described previously (Liu et al., 2020; Wang et al.,  
255 2020; Wang et al., 2021).

256 An end-point-dilution microplate neutralization assay was performed to measure the  
257 neutralization activity of convalescent plasma samples, vaccinee sera, and purified  
258 mAbs. Triplicates of each dilution were incubated with SARS-CoV-2 at an MOI of 0.1 in  
259 EMEM with 7.5% inactivated fetal calf serum (FCS) for 1 hour at 37°C. Post incubation,  
260 the virus-antibody mixture was transferred onto a monolayer of Vero E6 cells grown  
261 overnight. The cells were incubated with the mixture for ~70 hrs. CPE was visually  
262 scored for each well in a blinded fashion by two independent observers. The results  
263 were then converted into percentage neutralization at a given sample dilution or mAb  
264 concentration, and the averages  $\pm$  SEM were plotted using a five-parameter dose-  
265 response curve in GraphPad Prism.

### 266 **Cryo-EM data collection and processing**

267 2 $\mu$ L P.1 spike protein at a concentration of 2 mg/ml was incubated in 10 mM Hepes pH  
268 7.4, 150 mM NaCl, and 0.005% n-dodecyl- $\beta$ -D-maltoside (DDM) was incubated on C-  
269 flat 1.2/1.3 carbon grids for 30 seconds and vitrified using a Vitrobot plunge freezer.  
270 Data were collected on a Titan Krios electron microscope operating at 300 kV, equipped  
271 with a Gatan K3 direct electron detector and energy filter, using the Legimon software  
272 package (Suloway et al., 2005). A total electron fluence of 51.69 e-/Å<sup>2</sup> was fractionated

273 over 40 frames, with a total exposure time of 2.0 seconds. A magnification of 81,000x  
274 resulted in a pixel size of 1.058 Å, and a defocus range of -0.4 to -3.5 µm was used.

275

276 All processing was done using cryoSPARC v2.15.0 (Punjani et al., 2017). Raw movies  
277 were aligned and dose-weighted using patch motion correction, and the CTF was  
278 estimated using patch CTF estimation. A small subset of approximately 200  
279 micrographs were picked using blob picker, followed by 2D classification and manual  
280 curation of particle picks, and used to train a Topaz neural network. This network was  
281 then used to pick particles from the remaining micrographs, which were extracted with a  
282 box size of 384 pixels.

283

#### 284 **Cryo-EM model building**

285 We used PDB 6XM0, one of the most complete coronavirus spike structures, as a  
286 starting model. The model was docked to the map using Chimera. The model was then  
287 fitted interactively using COOT (Emsley and Cowtan, 2004) with real space refinement  
288 performed in Phenix 1.18 (Adams et al., 2004). Validation was performed using  
289 Molprobity (Davis et al., 2004) and EMRinger (Barad et al., 2015). The model was  
290 submitted to the PDB with PDB ID XXX. Figures were prepared using UCSF ChimeraX  
291 (Goddard et al., 2018).

292 **Figure S1. Neutralization of BZ $\Delta$ 10 and P.1 by mAbs, convalescent plasma, and**  
293 **vaccinee sera.** Related to Figure 1

294 (A) Neutralization of WT and BZ $\Delta$ 10 pseudoviruses, and WA1 and P.1 authentic viruses  
295 by anti-RBD mAbs.

296 (B) Neutralization of WT, BZ $\Delta$ 10, and single-mutation pseudoviruses, and WA1 and P.1  
297 authentic viruses by anti-NTD mAbs.

298 (C) Neutralization of WT and BZ $\Delta$ 10 pseudoviruses, and WA1 and P.1 authentic viruses  
299 by convalescent plasma.

300 (D) Neutralization of WT and BZ $\Delta$ 10 pseudoviruses, and WA1 and P.1 authentic viruses  
301 by vaccinee sera.

302 Data represent mean  $\pm$  SEM of technical triplicates.

303

304 **Figure S2. Cryo-EM Data Collection and Refinement.** Related to Figure 2

305 (A) Representative micrograph, power spectrum, and contrast transfer function (CTF) fit.

306 (B) Representative 2D class averages showing spike particles.

307 (C) Global consensus refinement Fourier Shell Correlation (FSC) curve and particle  
308 projection viewing angle distribution.

309 (D) Local resolution estimation mapped on surface density for global refinement.

310

311 **Table S1. Cryo-EM Data Collection and Refinement Statistics.** Related to Figure 2

312

313 **Video S1. Cryosparc 3D-variability analysis of the P1 spike.** Related to Figure 2

314

## 315 References

- 316 Adams, P.D., Gopal, K., Grosse-Kunstleve, R.W., Hung, L.W., Ioerger, T.R., McCoy, A.J., Moriarty,  
317 N.W., Pai, R.K., Read, R.J., Romo, T.D., *et al.* (2004). Recent developments in the PHENIX  
318 software for automated crystallographic structure determination. *J Synchrotron Radiat* **11**, 53-  
319 55.
- 320 Anderson, E.J., Roupael, N.G., Widge, A.T., Jackson, L.A., Roberts, P.C., Makhene, M., Chappell,  
321 J.D., Denison, M.R., Stevens, L.J., Pruijssers, A.J., *et al.* (2020). Safety and Immunogenicity of  
322 SARS-CoV-2 mRNA-1273 Vaccine in Older Adults. *N Engl J Med* **383**, 2427-2438.
- 323 Annavajhala, M.K., Mohri, H., Zucker, J.E., Sheng, Z., Wang, P., Gomez-Simmonds, A., Ho, D.D.,  
324 and Uhlemann, A.-C. (2021). A Novel SARS-CoV-2 Variant of Concern, B.1.526, Identified in New  
325 York. Preprint at  
326 <https://www.medrxiv.org/content/medrxiv/early/2021/2002/2025/2021.2002.2023.21252259>.
- 327 Barad, B.A., Echols, N., Wang, R.Y., Cheng, Y., DiMaio, F., Adams, P.D., and Fraser, J.S. (2015).  
328 EMRinger: side chain-directed model and map validation for 3D cryo-electron microscopy. *Nat*  
329 *Methods* **12**, 943-946.
- 330 Cerutti, G., Guo, Y., Zhou, T., Gorman, J., Lee, M., Rapp, M., Reddem, E.R., Yu, J., Bahna, F.,  
331 Bimela, J., *et al.* (2021). Potent SARS-CoV-2 Neutralizing Antibodies Directed Against Spike N-  
332 Terminal Domain Target a Single Supersite. Preprint at  
333 <https://www.biorxiv.org/content/biorxiv/early/2021/2001/2011/2021.2001.2010.426120>.
- 334 Chen, P., Nirula, A., Heller, B., Gottlieb, R.L., Boscia, J., Morris, J., Huhn, G., Cardona, J.,  
335 Mocherla, B., Stosor, V., *et al.* (2021). SARS-CoV-2 Neutralizing Antibody LY-CoV555 in  
336 Outpatients with Covid-19. *N Engl J Med* **384**, 229-237.
- 337 Davis, I.W., Murray, L.W., Richardson, J.S., and Richardson, D.C. (2004). MOLPROBITY: structure  
338 validation and all-atom contact analysis for nucleic acids and their complexes. *Nucleic Acids Res*  
339 **32**, W615-619.
- 340 Emsley, P., and Cowtan, K. (2004). Coot: model-building tools for molecular graphics. *Acta*  
341 *Crystallogr D Biol Crystallogr* **60**, 2126-2132.
- 342 Faria, N.R. (2021). Genomic characterisation of an emergent SARS-CoV-2 lineage in Manaus:  
343 preliminary findings. <https://virological.org/t/genomic-characterisation-of-an-emergent-sars-cov-2-lineage-in-manaus-preliminary-findings/586>
- 345 Garcia-Beltran, W.F., Lam, E.C., Denis, K.S., Nitido, A.D., Garcia, Z.H., Hauser, B.M., Feldman, J.,  
346 Pavlovic, M.N., Gregory, D.J., Poznansky, M.C., *et al.* (2021). Circulating SARS-CoV-2 variants  
347 escape neutralization by vaccine-induced humoral immunity. Preprint at  
348 <https://www.medrxiv.org/content/medrxiv/early/2021/2002/2018/2021.2002.2014.21251704>.
- 349 Goddard, T.D., Huang, C.C., Meng, E.C., Pettersen, E.F., Couch, G.S., Morris, J.H., and Ferrin, T.E.  
350 (2018). UCSF ChimeraX: Meeting modern challenges in visualization and analysis. *Protein Sci* **27**,  
351 14-25.
- 352 Gottlieb, R.L., Nirula, A., Chen, P., Boscia, J., Heller, B., Morris, J., Huhn, G., Cardona, J.,  
353 Mocherla, B., Stosor, V., *et al.* (2021). Effect of Bamlanivimab as Monotherapy or in  
354 Combination With Etesevimab on Viral Load in Patients With Mild to Moderate COVID-19: A  
355 Randomized Clinical Trial. *JAMA* **325**, 632-644.
- 356 Hansen, J., Baum, A., Pascal, K.E., Russo, V., Giordano, S., Wloga, E., Fulton, B.O., Yan, Y., Koon,  
357 K., Patel, K., *et al.* (2020). Studies in humanized mice and convalescent humans yield a SARS-  
358 CoV-2 antibody cocktail. *Science* **369**, 1010-1014.



359 Korber, B., Fischer, W.M., Gnanakaran, S., Yoon, H., Theiler, J., Abfalterer, W., Hengartner, N.,  
360 Giorgi, E.E., Bhattacharya, T., Foley, B., *et al.* (2020). Tracking Changes in SARS-CoV-2 Spike:  
361 Evidence that D614G Increases Infectivity of the COVID-19 Virus. *Cell* 182, 812-827 e819.  
362 Liu, L., Wang, P., Nair, M.S., Yu, J., Rapp, M., Wang, Q., Luo, Y., Chan, J.F., Sahi, V., Figueroa, A.,  
363 *et al.* (2020). Potent neutralizing antibodies against multiple epitopes on SARS-CoV-2 spike.  
364 *Nature* 584, 450-456.  
365 Liu, Y., Liu, J., Xia, H., Zhang, X., Fontes-Garfias, C.R., Swanson, K.A., Cai, H., Sarkar, R., Chen, W.,  
366 Cutler, M., *et al.* (2021). Neutralizing Activity of BNT162b2-Elicited Serum - Preliminary Report.  
367 *N Engl J Med*, doi: 10.1056/NEJMc2102017. Online ahead of print.  
368 Naveca, F. (2021). Phylogenetic relationship of SARS-CoV-2 sequences from Amazonas with  
369 emerging Brazilian variants harboring mutations E484K and N501Y in the Spike protein.  
370 [https://virological.org/t/phylogenetic-relationship-of-sars-cov-2-sequences-from-amazonas-](https://virological.org/t/phylogenetic-relationship-of-sars-cov-2-sequences-from-amazonas-with-emerging-brazilian-variants-harboring-mutations-e484k-and-n501y-in-the-spike-protein/585)  
371 [with-emerging-brazilian-variants-harboring-mutations-e484k-and-n501y-in-the-spike-](https://virological.org/t/phylogenetic-relationship-of-sars-cov-2-sequences-from-amazonas-with-emerging-brazilian-variants-harboring-mutations-e484k-and-n501y-in-the-spike-protein/585)  
372 [protein/585](https://virological.org/t/phylogenetic-relationship-of-sars-cov-2-sequences-from-amazonas-with-emerging-brazilian-variants-harboring-mutations-e484k-and-n501y-in-the-spike-protein/585).  
373 Pinto, D., Park, Y.-J., Beltramello, M., Walls, A.C., Tortorici, M.A., Bianchi, S., Jaconi, S., Culap, K.,  
374 Zatta, F., De Marco, A., *et al.* (2020). Cross-neutralization of SARS-CoV-2 by a human  
375 monoclonal SARS-CoV antibody. *Nature* 583, 290-295.  
376 Polack, F.P., Thomas, S.J., Kitchin, N., Absalon, J., Gurtman, A., Lockhart, S., Perez, J.L., Perez  
377 Marc, G., Moreira, E.D., Zerbini, C., *et al.* (2020). Safety and Efficacy of the BNT162b2 mRNA  
378 Covid-19 Vaccine. *N Engl J Med* 383, 2603-2615.  
379 Punjani, A., Rubinstein, J.L., Fleet, D.J., and Brubaker, M.A. (2017). cryoSPARC: algorithms for  
380 rapid unsupervised cryo-EM structure determination. *Nat Methods* 14, 290-296.  
381 Robbiani, D.F., Gaebler, C., Muecksch, F., Lorenzi, J.C.C., Wang, Z., Cho, A., Agudelo, M., Barnes,  
382 C.O., Gazumyan, A., Finkin, S., *et al.* (2020). Convergent antibody responses to SARS-CoV-2 in  
383 convalescent individuals. *Nature* 584, 437-442.  
384 Shi, R., Shan, C., Duan, X., Chen, Z., Liu, P., Song, J., Song, T., Bi, X., Han, C., Wu, L., *et al.* (2020).  
385 A human neutralizing antibody targets the receptor-binding site of SARS-CoV-2. *Nature* 584,  
386 120-124.  
387 Suloway, C., Pulokas, J., Fellmann, D., Cheng, A., Guerra, F., Quispe, J., Stagg, S., Potter, C.S., and  
388 Carragher, B. (2005). Automated molecular microscopy: the new Legimon system. *J Struct Biol*  
389 151, 41-60.  
390 Tegally, H., Wilkinson, E., Giovanetti, M., Iranzadeh, A., Fonseca, V., Giandhari, J., Doolabh, D.,  
391 Pillay, S., San, E.J., Msomi, N., *et al.* (2021). Emergence of a SARS-CoV-2 variant of concern with  
392 mutations in spike glycoprotein. *Nature*.  
393 Wang, P., Liu, L., Nair, M.S., Yin, M.T., Luo, Y., Wang, Q., Yuan, T., Mori, K., Solis, A.G.,  
394 Yamashita, M., *et al.* (2020). SARS-CoV-2 neutralizing antibody responses are more robust in  
395 patients with severe disease. *Emerg Microbes Infect* 9, 2091-2093.  
396 Wang, P., Nair, M.S., Liu, L., Iketani, S., Luo, Y., Guo, Y., Wang, M., Yu, J., Zhang, B., Kwong, P.D.,  
397 *et al.* (2021). Antibody Resistance of SARS-CoV-2 Variants B.1.351 and B.1.1.7. *Nature*, In press.  
398 West, A.P., Barnes, C.O., Yang, Z., and Bjorkman, P.J. (2021). SARS-CoV-2 lineage B.1.526  
399 emerging in the New York region detected by software utility created to query the spike  
400 mutational landscape. Preprint at  
401 <https://www.biorxiv.org/content/biorxiv/early/2021/2002/2023/2021.2002.2014.431043>.

402 Wu, K., Werner, A.P., Koch, M., Choi, A., Narayanan, E., Stewart-Jones, G.B.E., Colpitts, T.,  
403 Bennett, H., Boyoglu-Barnum, S., Shi, W., *et al.* (2021). Serum Neutralizing Activity Elicited by  
404 mRNA-1273 Vaccine - Preliminary Report. *N Engl J Med*, doi: 10.1056/NEJMc2102179. Online  
405 ahead of print.

406 Yurkovetskiy, L., Wang, X., Pascal, K.E., Tomkins-Tinch, C., Nyalile, T.P., Wang, Y., Baum, A.,  
407 Diehl, W.E., Dauphin, A., Carbone, C., *et al.* (2020). Structural and Functional Analysis of the  
408 D614G SARS-CoV-2 Spike Protein Variant. *Cell* 183, 739-751 e738.

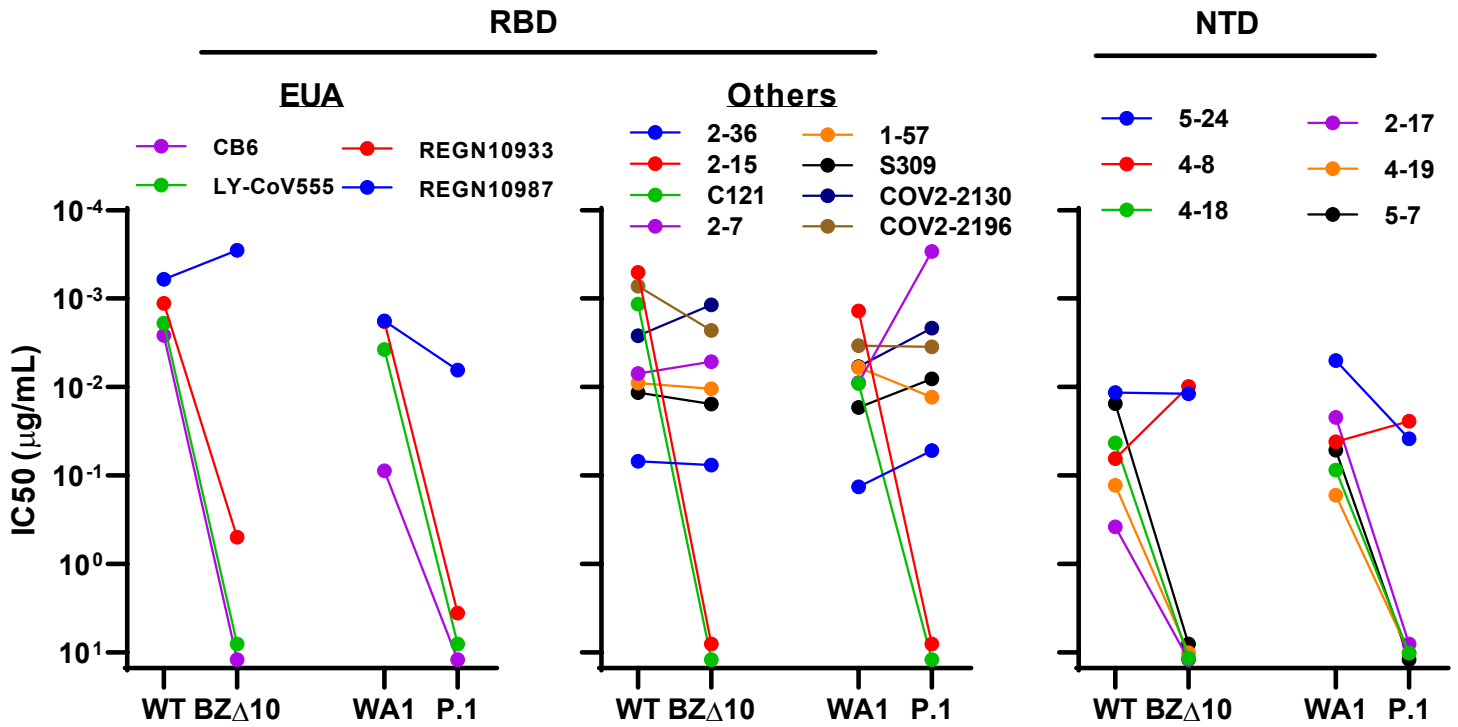
409 Zhou, T., Tsybovsky, Y., Gorman, J., Rapp, M., Cerutti, G., Chuang, G.Y., Katsamba, P.S.,  
410 Sampson, J.M., Schon, A., Bimela, J., *et al.* (2020). Cryo-EM Structures of SARS-CoV-2 Spike  
411 without and with ACE2 Reveal a pH-Dependent Switch to Mediate Endosomal Positioning of  
412 Receptor-Binding Domains. *Cell Host Microbe* 28, 867-879 e865.

413 Zost, S.J., Gilchuk, P., Case, J.B., Binshtein, E., Chen, R.E., Nkolola, J.P., Schafer, A., Reidy, J.X.,  
414 Trivette, A., Nargi, R.S., *et al.* (2020). Potently neutralizing and protective human antibodies  
415 against SARS-CoV-2. *Nature* 584, 443-449.

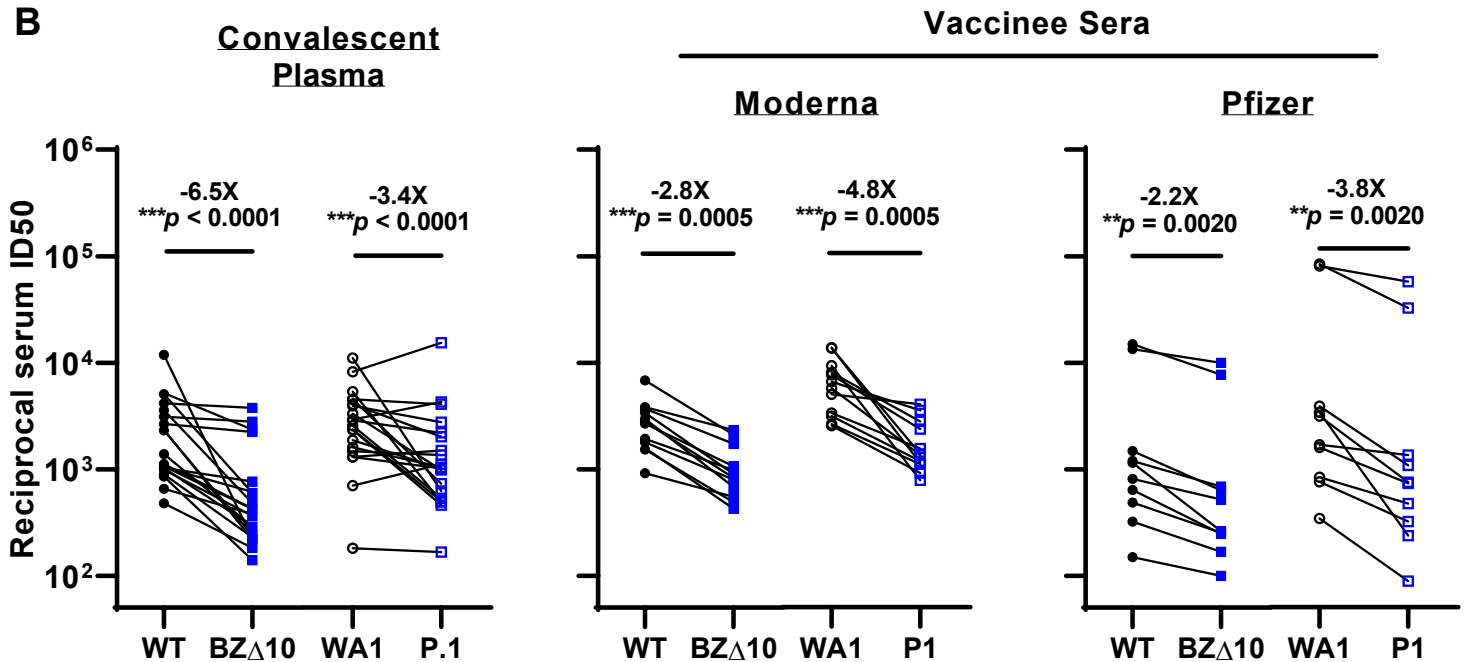
416

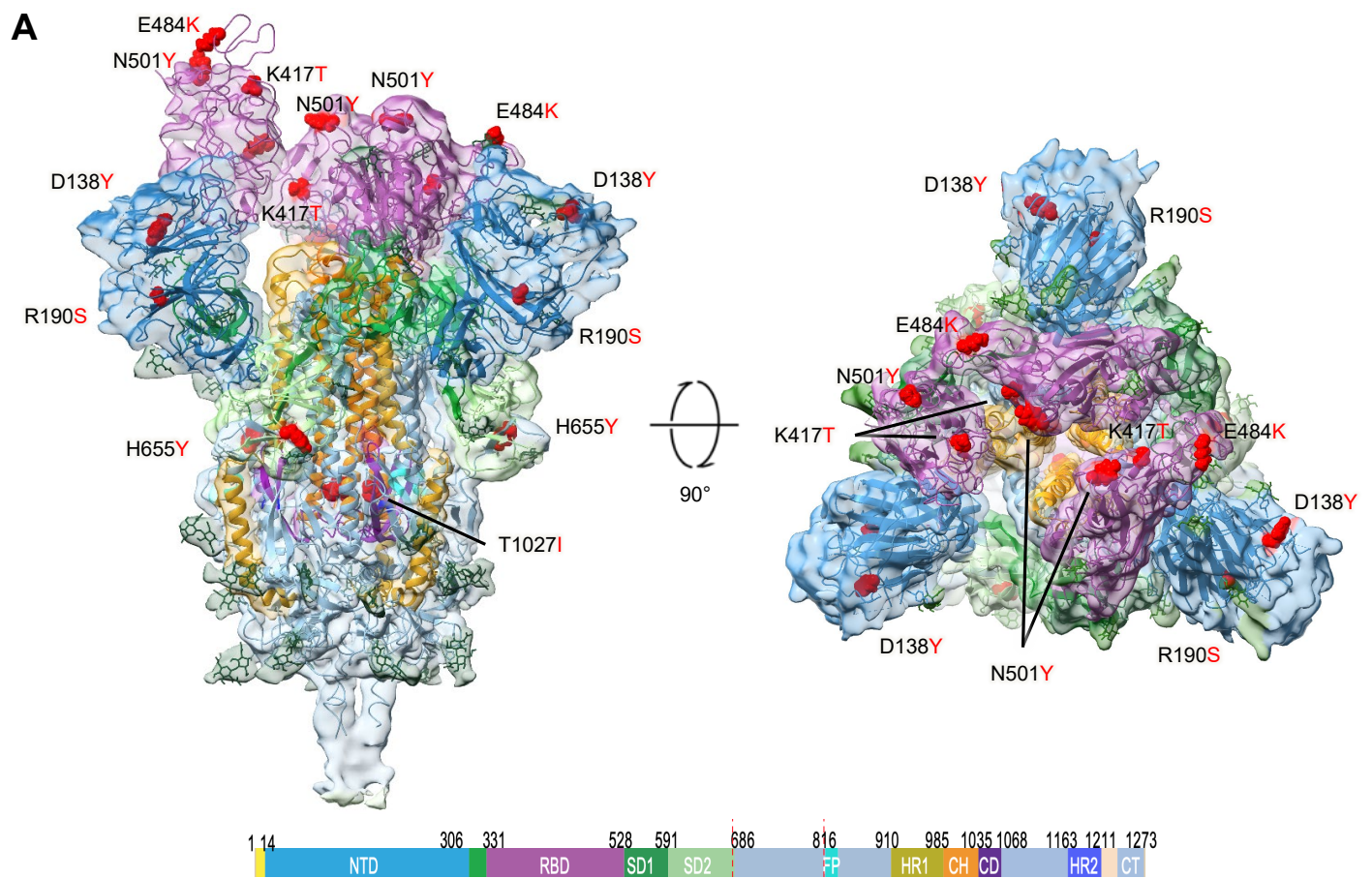
**A**

**Monoclonal Antibodies**

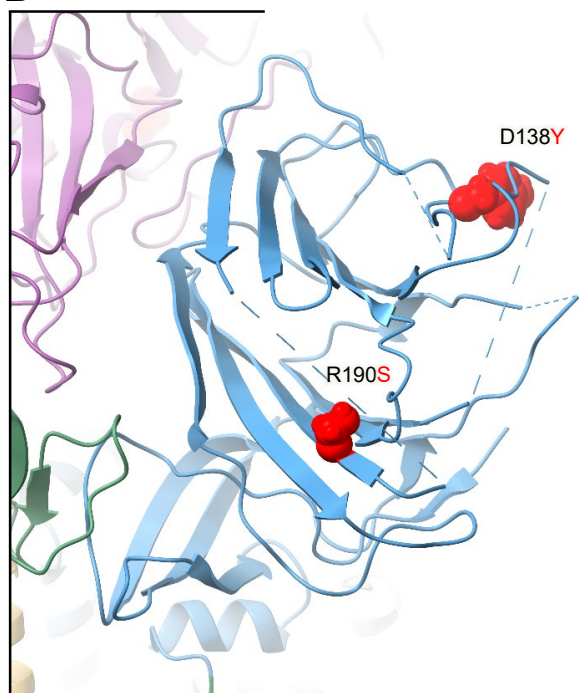


**B**





**B** NTD details



**C** RBD details

